

Effects of Pore Position in Depth on Stress/Strain Concentration and Fatigue Crack Initiation

ZHIQIANG XU, WEI WEN, and TONGGUANG ZHAI

The stress field around a pore was analyzed as a function of the pore position in depth in the surface of a linear elastic solid using finite element modeling. It was found that the pore depth dominated the stress field around the pore on the surface and that the maximum stress was increased sharply when the pore intercepted with the surface at its top. Given the applied nominal stress, the magnitude of the maximum main stress only depended on the relative depth of the pore, while the pore size affected the stress distribution in the surface. An elastic-plastic model was also used to account for the yielding effect in the region where stress was over the yield strength. The results still indicated a significant maximum stress concentration when the pore was just buried underneath the surface, but with a lowered value than that of the linear elastic model. These results were consistent with the experimental observations that fatigue cracks were preferably initiated from pores and particles, which were just intercepted at their top with the sample surface or just buried beneath the surface.

DOI: 10.1007/s11661-011-0947-x

© The Minerals, Metals & Materials Society and ASM International 2011

I. INTRODUCTION

THE Al alloy castings are widely used in engineering applications, such as engine blocks, gear boxes, vehicle wheels, gearbox cases, fan hubs, *etc.*, because of their relatively high specific strength and low cost. Since these Al components are often under dynamic loading in service, their fatigue properties become critical for the structural integrity of an entire engineering system that uses these components. Since Al castings inevitably contain porosities and coarse particles or inclusions, which are detrimental to their fatigue properties, it is always desirable to try to reduce the number and size of the porosities in the castings. Effective methods can be developed to reduce these detrimental pores, only by fully and quantitatively understanding all the factors that control fatigue damage around pores in these castings.

It has been recognized that the fatigue life of an Al alloy casting is often one to two orders of magnitude lower than that of the same alloy without cast defects.^[1] Among these cast defects, gas pores are the most detrimental ones at which fatigue cracks are often initiated prematurely.^[1-6] In cast alloys, it is generally believed that cracks are initiated from the largest pores, because these pores could cause the highest stress concentration around them. Therefore, the larger these pores are, the more inferior the fatigue properties in the alloys containing the pores. Although the pores in the

surface region are the preferred sites for fatigue crack initiation, cracks are only initiated from a small percentage of the pores existing on the surface. In 713 Al alloy castings, it has been found that only 1.4 pct of the pores on the sample surface led to fatigue crack initiation, and that cracks are not necessarily initiated from the larger pores on the surface.^[7] In the case of wrought alloys, in which coarse particles are the preferred sites for fatigue crack initiation, only about 4 pct of the particles on the surface could cause crack initiation in an AA7075 Al alloy.^[8] Moreover, previous work also indicated that fatigue cracks were most likely to be initiated from those pores that were just buried beneath the surface.^[9,10] Fan *et al.* analyzed the plastic shear strain range as a function of the distance between a pore and the free surface with a finite element analysis method, and found that the plastic shear strain range increased with the decrease in distance between the pore and the free surface.^[11] A modified Manson–Coffin law was used to calculate the life for fatigue crack initiation using the plastic shear strain range, indicating that the crack initiation life decreased with the decrease in the pore-surface distance. The stress and strain fields were also analyzed, using a finite element analysis method, around the pores with different diameters ($\geq 100 \mu\text{m}$) but at some fixed distances from the free surface.^[12] The work showed that the stress concentration factor varied significantly with the pore location, only when the pore diameter was over $200 \mu\text{m}$. More detailed work performed later indicated that the stress/strain concentrations reached their peaks when a pore of $200 \mu\text{m}$ in diameter was just buried beneath the surface.^[13] Further work still needs to be done to thoroughly understand how the size, shape, orientation, and relative location to the surface of a pore could control the stress and strain fields, when the pore is smaller than $200 \mu\text{m}$ in diameter, with a view to identifying the fatigue crack initiation

ZHIQIANG XU, Professor, is with the College of Mechanical Engineering, Yanshan University, Qinhuangdao, Hebei 066004, P.R. China. WEI WEN, Graduate Student, and TONGGUANG ZHAI, Associate Professor, are with the Department of Chemical and Materials Engineering, University of Kentucky, Lexington, KY 40506. Contact e-mail: tzhai@engr.uky.edu

Manuscript submitted March 28, 2011.

Article published online November 11, 2011

sites from the pores in the surface in the alloys with pores.

In this article, the stress field around a pore in the surface was quantified using finite element analysis with regard to the pore size and position in depth. The results from the work revealed that the stress field was more sensitive to the pore location in the surface, and that the stress concentration reached the maximum value when the pore was just buried beneath the surface.

II. FINITE ELEMENT MODELING

The matrix of the alloy simulated in this work was assumed to be continuous, homogenous, and linear elastic. As shown in Figure 1(a), the alloy in a shape of half a cylinder, which was $360\ \mu\text{m}$ in diameter and $360\ \mu\text{m}$ in length, had the free surface (X - Z plane) along the axis (*i.e.*, X -axis) of the cylinder. The Y -axis was normal to the free surface of the alloy. A spherical pore, $30\ \mu\text{m}$ in diameter, was located in the surface in the middle of the alloy. The distance between the pore center and the alloy free surface was D , and the pore radius was r (Figure 1(b)). When the pore center was outside the surface, D was negative; otherwise, it was positive. With $D/r = -1, 0,$ and 1 , the pore was located just completely outside the surface, half inside the alloy, and just totally inside the alloy, respectively. A tensile stress σ_0 of $103\ \text{MPa}$ was applied along the axis of the cylinder. Since the size of the pore was far smaller than that of the cylinder, the stress was assumed to be uniformly applied to the pore. Because of the symmetry of the pore, only a quarter of the pore in a quarter of the alloy was used in the finite element model for stress analysis in this work (Figure 1), to minimize the calculation time. The alloy

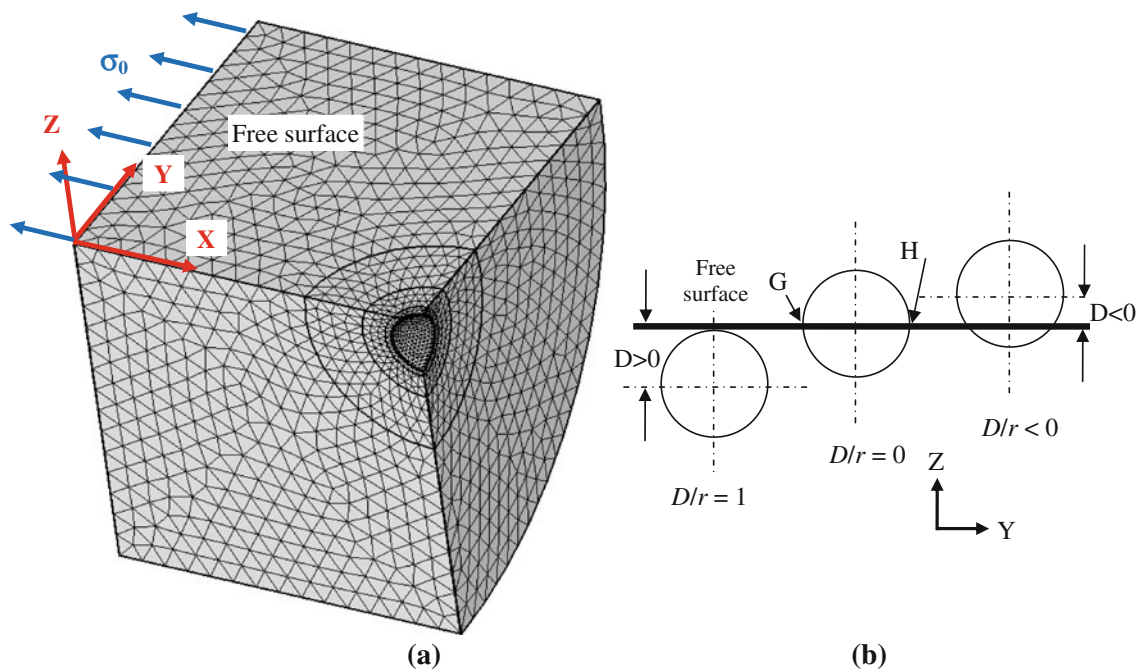


Fig. 1—(a) Finite element model for a pore in the surface. (b) Typical locations of the pore in the surface.

was assumed to be a cast 713 Al-Zn alloy, which had a yield strength of $122\ \text{MPa}$, Young's modulus of $61\ \text{GPa}$, and Poisson ratio of 0.3 . The stress-strain relationship was measured from tensile tests at room temperature. When the stress field calculated using a linear elastic model around the pore was over the yield strength, an elastic-plastic model was then used to quantify the stress field. The shape of the elements was tetrahedral with the size of $0.5\ \mu\text{m}$ close to the pore. The size of the tetrahedrons was subsequently increased gradually away from the pore, from $1\ \mu\text{m}$ and 2 to $5\ \mu\text{m}$.

III. RESULTS AND DISCUSSION

A. The Effect of Pore Position in Depth

The maximum principal stress, σ_1 , was quantified around the pore with a radius of $15\ \mu\text{m}$ at different

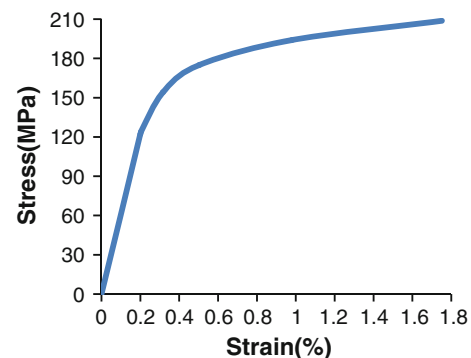


Fig. 2—Tensile stress-strain curve measured in a cast 713 Al-Zn alloy.

depths relative to the sample free surface, assuming the alloy matrix was linear elastic, homogeneous, and continuous. Figure 3 shows the distribution of the stress concentration factor, $k_t = \sigma_1/\sigma_0$, at $D/r = 0$ and 0.9, respectively, as an example. Stress concentration generally occurred in the region along the line that was perpendicular to the load axis X on the pore surface, as shown in Figure 3(a). The maximum stress appeared at the intercept points (*i.e.*, points G and H) between this line and the alloy surface (Figure 1(b)), and its value varied significantly with the depth of the pore in the surface region. As shown in Figure 4, the maximum stress concentration factor increased sharply at $D/r = 1$, *i.e.*, when the pore intercepted with the surface at its top. When half or less than half of the pore was in the alloy, *i.e.*, $D/r \leq 0$, the maximum stress concentration factor was 2 or less than 2, whereas it was larger than 2 when more than half of the pore was in the alloy or completely buried beneath the surface within a distance of one diameter in depth ($0 \leq D/r \leq 2$). This indicated that only those pores located between $D/r = 0$ and 2 were more likely to cause crack initiation in the alloy, since they resulted in higher stress concentration on the surface. The diameter (normalized by the pore radius) of the pore on the alloy free surface was also plotted as a function of D/r in Figure 4. It can be seen in Figure 4 that the pore size on the surface varies with the pore depth, and that those pores that have a high K_t do not have a large size on the surface. This is consistent with the experimental observations that fatigue cracks are often initiated from the pores that are relatively small in size on the surface (Figure 5(a)) and sometimes from subsurface pores (Figure 5(b)) in a cast 713 Al alloy.^[7] This may also qualitatively explain why only a small percentage, *i.e.*, 1.4 pct in the cast 713 Al alloy, of the pores found on the surface could cause fatigue crack

initiation, since the percentage of those pores that are just buried beneath the surface or intercepted at their top parts by the surface is small.

Because of the stress concentration around the pore, local yielding could take place in the alloy. As a result, the elastic-plastic model had to be used to quantify the stress concentration factor, K_t , by taking into account the measured flow stress-strain relationship in Figure 2. The so-calculated K_t was also plotted in Figure 4. Due to the plastic deformation, which could release the stress concentration, there is only a narrow spike at $D/r = 1$ in the so-calculated K_t -depth curve in Figure 4. With the elastic-plastic model, the maximum principal plastic

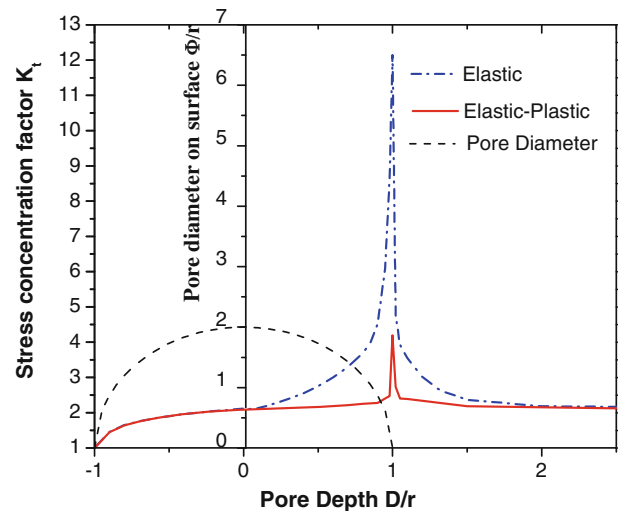


Fig. 4—Maximum stress concentration and the pore surface diameter as a function of the pore position in depth, which is normalized by the pore radius.

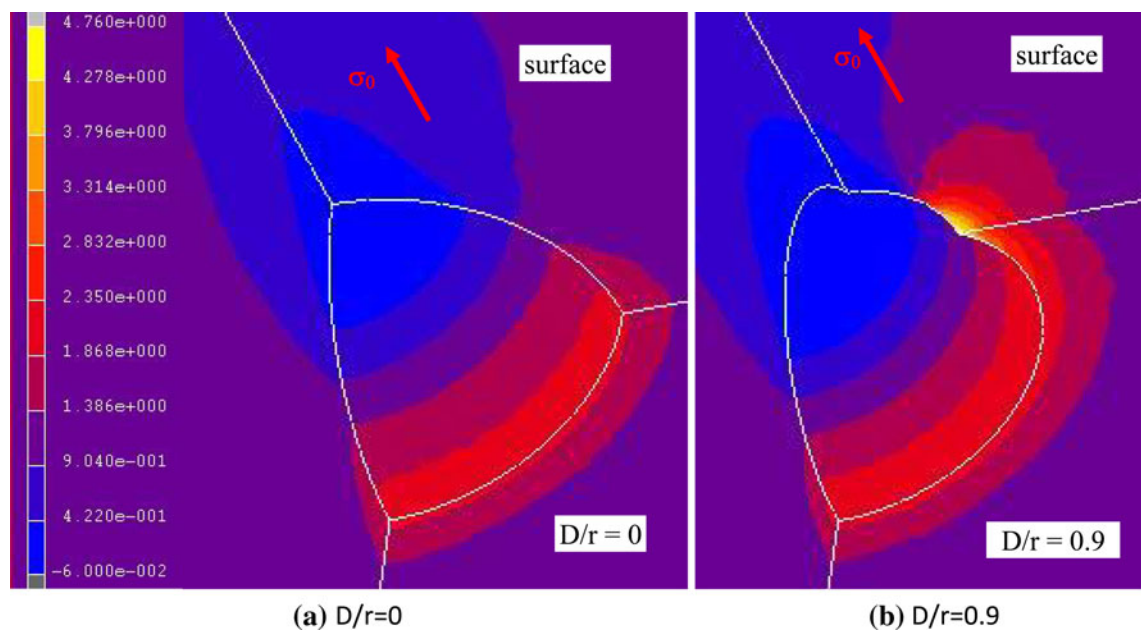


Fig. 3—Distribution of the stress concentration factor around (a) a pore intercepting the surface in the middle ($D/r = 0$) and (b) a pore at $D/r = 0.9$.

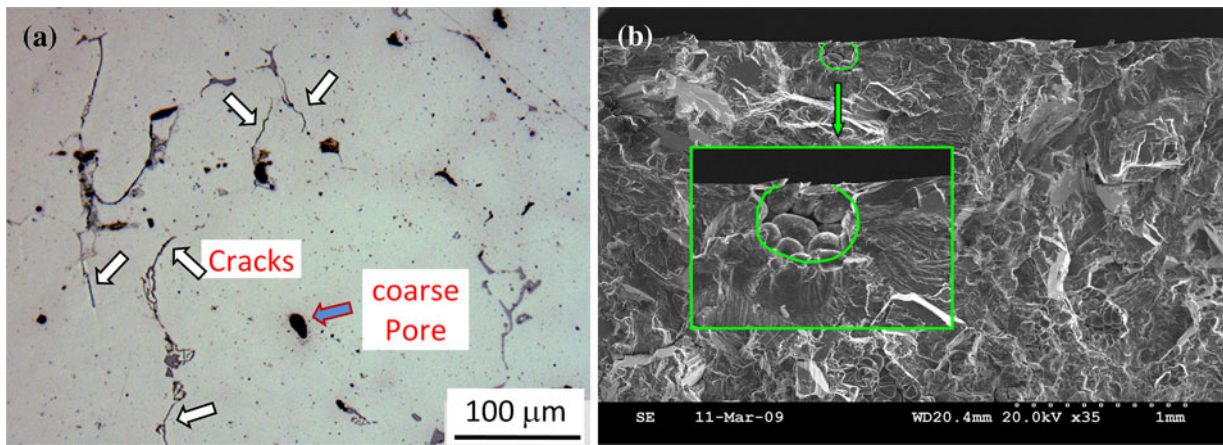


Fig. 5—(a) Optical micrograph of cracks. (b) SEM micrograph showing the fatigue fracture surface where the crack is initiated from the pore that intercepts with the surface in the cast 713 Al-Zn alloy.^[7]

shear strain was quantified around the pore under the uniaxial tension of 103 MPa. Figure 6 is the distribution of the maximum principal plastic shear strain around the pore at $D/r = 0.9$, as an example. It is evident in Figure 6 that there is a significant strain concentration in the region along the line perpendicular to the load axis on the pore surface, with the maximum shear plastic strain being at points G and H. The strain concentration occurred in the same region as that for the stress concentration predicted by the elastic model in Figure 3(b). Although these results were obtained for the case of static loading, they should still be true for the case of cyclic loading, since the cyclic plastic strain concentration should also occur at the same location as those in the case of static loading. It has been recognized that shear plastic strain is the main driving force for fatigue crack initiation.^[14,15] This explains why fatigue cracks are often initiated preferably from the pores, which are located mostly or completely inside the alloy in the surface region at a cyclic stress much lower than the yield stress of the alloy,^[9,10] as shown in Figure 5(b), since such a pore causes significant strain concentration. Large shear plastic strain leads to early initiation of short fatigue cracks in the alloy.

Although obtained from a pore of 30 μm in diameter, the results shown in Figure 4 demonstrate that the stress and strain concentrations as a function of the pore location in the surface are independent of the size of the pore, since the distance between the pore and the surface is normalized by the pore radius. In other words, they are valid for spherical pores of any sizes in the surface. However, the results by Gao *et al.*^[12] showed that the stress concentration around a pore in the surface became less profound when the pore size was less than 200 μm in diameter. This discrepancy is attributed to the fact that the distances used in stress analysis by Gao *et al.* were fixed, *e.g.*, $D - r = -20, 20, 50, 100 \mu\text{m}$, *etc.*, for all the pores (with different diameters) considered in their work. As a result, the relative distances (D/r) between the pores and the surface were different for pores of different sizes; *i.e.*, they decreased with the increase in pore size. For example, for the smallest (100 μm) and largest (1000 μm) pores used in their

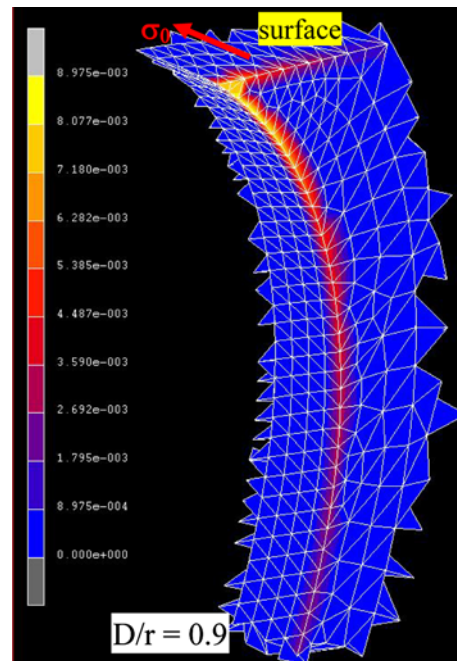


Fig. 6—Distribution of the maximum principal plastic shear strain along the line that is perpendicular to the load axis on the pore surface. $D/r = 0.9$, and $\sigma_0 = 103 \text{ MPa}$.

work, $D - r = -20, 20, 50, 100 \mu\text{m}$ are equivalent to $D/r = 0.8, 1.2, 1.5, 2.0$ and $D/r = 0.98, 1.02, 1.05, 1.1$, respectively. According to the results in Figure 4, the closer to 1 the relative distance D/r , the higher the stress concentration factor, for those D/r values used.

B. Effect of Pore Orientation

In this work, the effect of the orientation of an ellipsoidal pore on the stress field around the pore in the surface was analyzed using the finite element analysis method, since fatigue cracks are sometimes found to be initiated from ellipsoidal pores that are inclined in the surface, as shown in Figure 7. The alloy shown in Figure 7 is a cast A356 Al-Si alloy, which was fatigued

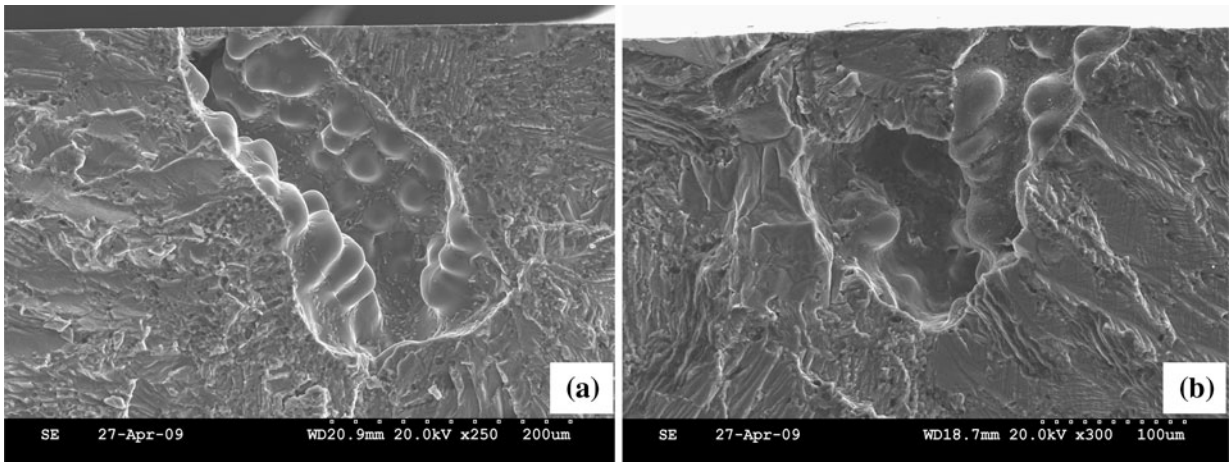


Fig. 7—SEM micrographs showing the fatigue fracture surface, where cracks are initiated from the elongated pores that are inclined in the surface in an A356-T6 Al-Si alloy.

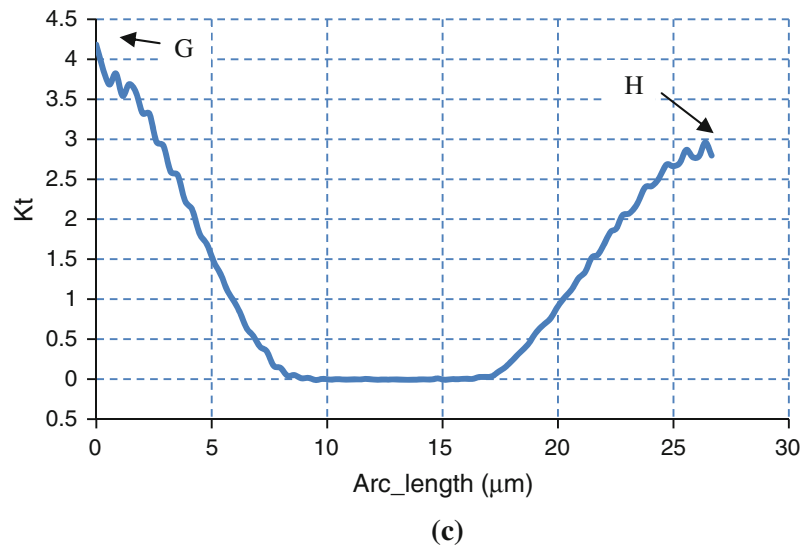
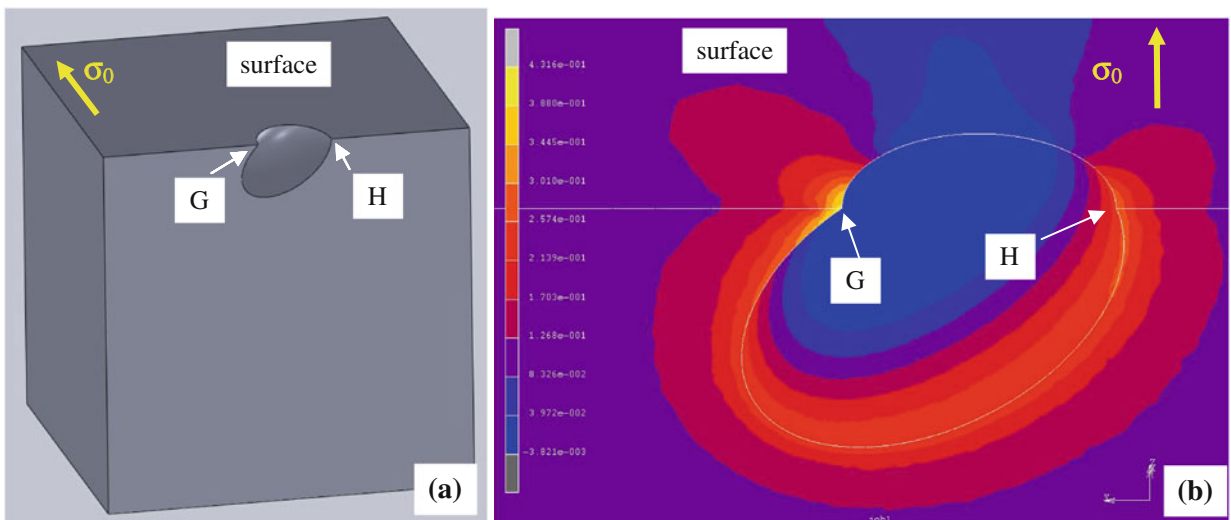


Fig. 8—(a) Schematic diagram showing an ellipsoidal pore inclined at an angle of 45 deg in the free surface. The radii in the three axes are 30, 20, and 20 μm , respectively. (b) Distribution of the stress concentration factor around the inclined ellipsoidal pore in the surface. (c) Distribution of the stress concentration factor, K_t , along the edge of the pore on the surface, as shown in (a).

in four-point bend. As shown in Figure 8(a), the pore with its three radii of 30, 20, and 20 μm , respectively, was inclined at an angle of 45 deg in the free surface. The applied stress, the alloy, and the finite element model used for the ellipsoidal pore were similar to those for the spherical pore discussed previously. The stress field around the ellipsoidal pore was then analyzed, and the maximum principal stress was used to calculate the stress concentration factor. Figure 8(b) shows the distribution of the stress concentration factor around the pore. Figure 8(c) is the profile of the stress concentration factor along the edge of the pore on the surface, as shown in Figure 8(a). It is evident in Figure 8(c) that the stress concentration factor (4.2) is much higher around point G, where the pore intercepts the surface at an acute angle, than that (3.0) around point H, where the pore intercepts the surface at an obtuse angle. This means that, by tilting the ellipsoidal pore, the stress field around the pore in the surface is further increased. This result is understandable since the cross-sectional area around point G is reduced faster toward the pore edge on the surface than around point H, resulting in higher stress concentration at point G than point H. As in the case of a spherical pore in Figure 6, there should also be significant shear plastic strain concentration in the region where the stress concentration takes place around the inclined pore. It is the shear plastic strain concentration that causes fatigue crack initiation in such a pore in the surface.

C. Effect of Pore Size

The Von Mises stress and effective strain were quantified along the line perpendicular to the load axis on the surface from the point where a spherical pore intercepted with the alloy surface, as illustrated in Figure 9(a). The Von Mises stresses and effective strains for pores of 15 and 75 μm in radius are given in Figures 9(b) and (c), respectively, assuming that the alloy was the cast 713 Al alloy and the applied stress of 103 MPa. It is evident that a larger pore did not necessarily cause larger maximum effective stress or strain but a much larger region for the same stress or strain concentration. Namely, a larger pore causes a larger stress/strain concentration zone around it than a smaller pore. For example, the region in which the effective stress is larger than 190 MPa is 30 μm for the pore of 75- μm radius, and it is about 7 μm for the pore with a radius of 15 μm . The region of effective strain larger than 1×10^{-2} is 30 μm for the pore of 75- μm radius (Figure 9(b)), while it is just about 6 μm for the pore of 15- μm radius (Figure 9(c)). The larger zone of high stress and strain concentration associated with larger pores is in agreement with the commonly observed results, that the larger the pores in an alloy, the lower the fatigue properties of the alloy.^[16] Although the results in Figure 4 are independent of the pore size, there should be a minimum value of the pore size below which the pores cannot effectively lead to fatigue crack

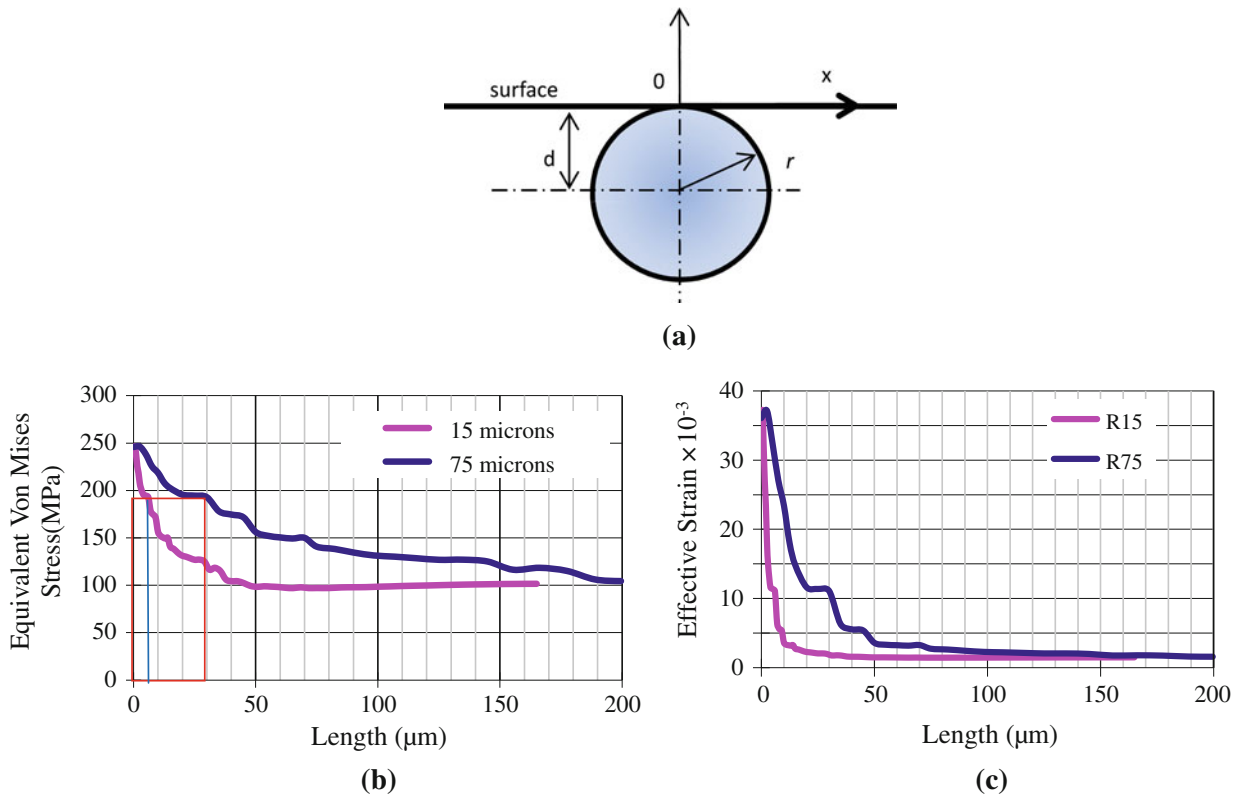
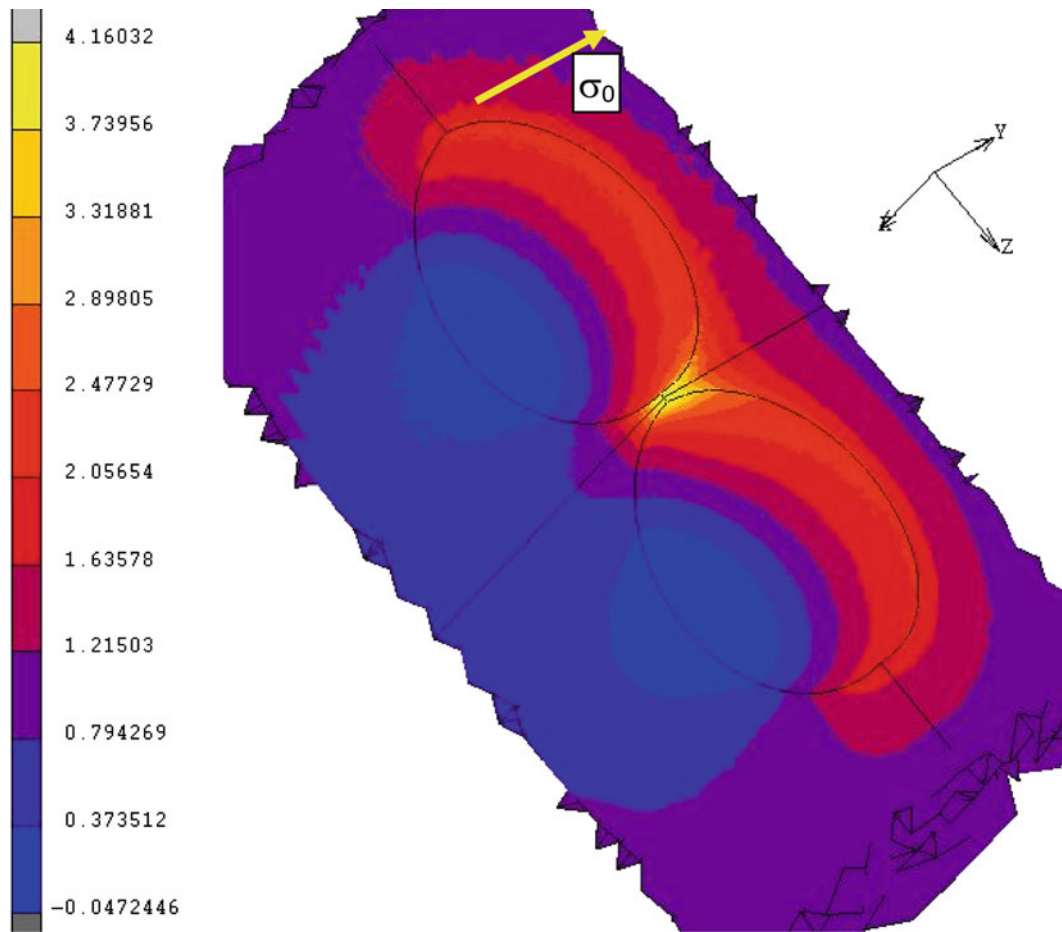
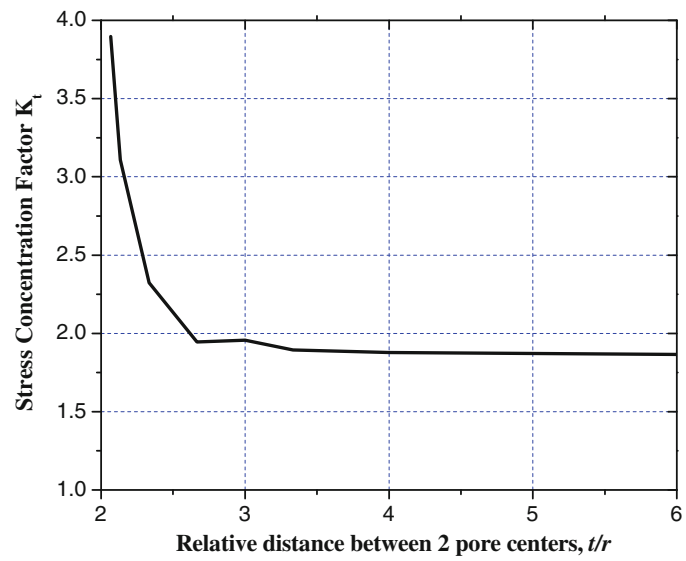


Fig. 9—(a) Sketch of a spherical pore intersecting the alloy surface at its top; O is the intercepting point. (b) Von Mises stress profiles along the line perpendicular to the load axis on the surface from the intercepting point O in (a), for pores of 15 and 75 μm in radius, respectively. (c) Effective strain profile along the line perpendicular to the load axis on the surface from the intercepting point O, for pores of 15 and 75 μm in radius, respectively.



(a)



(b)

Fig. 10—(a) Distribution of stress concentration factor around two pores $1\ \mu\text{m}$ apart in the direction perpendicular to the load axis. The radius of the pores is $15\ \mu\text{m}$. (b) Profile of the stress concentration factor as a function of the distance between the centers of two pores.

initiation, e.g., 15 μm in diameter for cast A356 Al alloys, as mentioned in Reference 11.

D. Effect of Pore Clustering

Since pores are sometimes clustered, leading to fatigue crack initiation, the effect of the pore clustering was investigated by analyzing the stress concentration factor around the two spherical pores of 15- μm radius using the finite element method. The two pores both intercepted at the half with the alloy surface and were 1 μm apart in the direction perpendicular to the load axis. Note that the case where two pores were aligned with the load axis was not considered here, because such a configuration was similar to that for a single pore. As shown in Figure 10, significant stress concentration takes place in the matrix on the surface between the pores. The maximum stress concentration factor, which is at the edge of the pore on the surface, as a function of the distance (t) between the two pores is plotted in Figure 10(b). The distance was between the centers of the two pores and normalized by the radius of the pores. The results in Figure 10(c) reveal that the stress concentration becomes significant when the two pores are within one radius away between the edges of the pores on the surface, i.e., $t/r \leq 3$. When the pores were more than one radius apart, the stress concentration was just the same as that of each individual pore. This means that pore clustering could promote fatigue crack initiation when two pores are within one radius apart in the direction perpendicular to the load axis.

IV. CONCLUSIONS

1. Significant stress and strain concentrations increased sharply when a pore intercepted the free surface of an alloy at its top. They became insignificant when less than half of the pore was inside the alloy or the pore was located deeper than one diameter of the pore from the free surface. This explained why fatigue cracks were often initiated from those pores that intercepted the free surface at the top halves or were completely buried beneath the surface within one radius in depth.
2. The pore size only increased the zone of high stress/strain concentration around the pore in the surface.
3. The stress/strain was further increased by tilting an elongated (ellipsoidal) pore in the surface. The stress/strain was much higher at the intercept point where the pore intercepted the free surface at an

acute angle than the intercept point at an obtuse angle.

4. The stress and strain concentrations were increased sharply with the decrease in distance between two pores in the surface, when they were within one radius apart in the direction perpendicular to the load axis. When the two pores were more than one radius apart, the stress and strain concentrations were the same as those for a single pore in the surface.

ACKNOWLEDGMENTS

Two of the authors (WW and TZ) were supported by the United States National Science Foundation through CAREER Award No. DMR-0645246. Professor Xu Zhiqiang was sponsored by the National Natural Science Foundation of China (Grant No. 50675187).

REFERENCES

1. H.R. Ammar, A.M. Samuel, and F.H. Samuel: *Mater. Sci. Eng. A*, 2008, vol. 473, pp. 65–75.
2. Q.G. Wang, D. Apelian, and D.A. Lados: *J. Light Met.*, 2001, vol. 1, pp. 73–84.
3. M.T. Todinov: *Mater. Sci. Eng. A*, 1998, vol. 255, pp. 117–23.
4. B. Atzori, G. Meneghetti, and L. Susmel: *Eng. Fract. Mech.*, 2004, vol. 71, pp. 759–68.
5. J. Linder, M. Axelsson, and H. Wilsson: *Int. J. Fatigue*, 2006, vol. 28, pp. 1752–58.
6. J.Z. Yi, Y.X. Gao, P.D. Lee, H.M. Flower, and T.C. Lindley: *Metall. Mater. Trans. A*, 2003, vol. 34A, pp. 1879–90.
7. Y.B. Zhang, J.H. Xu, and T. Zhai: *Mater. Sci. Eng. A*, 2010, vol. 527, pp. 3639–44.
8. J.E. Bozek, J.D. Hochhalter, M.G. Veilleux, M. Liu, G. Heber, S.D. Sintay, A.D. Rollett, D.J. Littlewood, A.M. Maniatty, H. Weiland, R.J. Christ, Jr., J. Payne, G. Welsh, D.G. Harlow, P.A. Wawrzynek, and A.R. Ingraffea: *Model. Simul. Mater. Sci. Eng.*, 2008, vol. 16, pp. 1–28.
9. S. Benedictus-deVries, A. Bakker, G.C.A.M. Janssen, and H. de Wit: *J. Eng. Mater. Technol.-Trans. ASEM*, 2004, 2004, vol. 126, pp. 199–203.
10. H.T. Pang and P.A.S. Reed: *Int. J. Fatigue*, 2003, vol. 25, pp. 1089–99.
11. J.H. Fan, D.L. McDowell, M.F. Horstemeyer, and K. Gall: *Eng. Fract. Mech.*, 2003, vol. 70, pp. 1281–1302.
12. Y.X. Gao, J.Z. Yi, P.D. Lee, and T.C. Lindley: *Fatigue Fract. Eng. Mater. Struct.*, 2004, vol. 27, pp. 559–70.
13. P. Li, P.D. Lee, D.M. Maijer, and T.C. Lindley: *Acta Mater.*, 2009, vol. 57, pp. 3539–48.
14. A. Fatemi and D. Socie: *Fatigue Fract. Eng. Mater. Struct.*, 1988, vol. 11, pp. 145–65.
15. D.L. McDowell: *Int. J. Fract.*, 1996, vol. 80, pp. 103–45.
16. M.J. Couper, A.E. Neeson, and J.R. Griffith: *Fatigue Fract. Mater. Struct.*, 1990, vol. 13, pp. 213–27.